ADVANCED ENERGY & SUSTAINABILITY RESEARCH
www.advenergysustres.com

The Influence of Electrolyte Formulation on Gas Evolution in Sodium-Ion Batteries with $NaMnO_2$ Cathode

*Siyu An, Barbara Nascimento Nunes, Rui Yao, Aleksandr Kondrakov, and Torsten Brezesinski**

Sodium-ion batteries (SIBs) are considered a promising alternative to lithium-ion batteries due to the high availability of sodium resources. Among the various candidates for the positive electrode, layered (O3-type) $NaMnO_2$ has attracted considerable attention. However, understanding of its interfacial stability remains limited. Differential electrochemical mass spectrometry (DEMS) is a powerful tool for monitoring gas evolution and therefore provides valuable insights into side reactions occurring at the interface between anode/cathode and electrolyte. In this work, the gassing behavior of SIB half-cells with $NaMnO_2$ cathode and six representative electrolyte formulations is investigated using DEMS. The results show that electrolytes with fluoroethylene carbonate effectively suppress parasitic reactions and promote the formation of passivating interphases, resulting in improved performance and limited gas release. PC-based electrolytes appear to be more stable than EC-based electrolytes, especially in combination with $NaClO_4$. The use of $NaPF_6$ is associated with increased H_2 evolution and possible manganese dissolution, thereby impairing interfacial stability and releasing more lattice oxygen. An increase in the upper cutoff potential enhances gas release, indicating more severe (electro)chemical oxidation of the electrolyte. Overall, this study paves the way for new strategies for tailoring electrolytes to improve the cyclability and safety of SIBs.

1. Introduction

The widespread use of lithium-ion batteries (LIBs) in areas such as portable electronic devices, electric vehicles, and stationary storage systems plays an important role in maintaining and further developing the functionality of today's society.[1–3] At the same time, the use of LIBs not only enables the redistribution of renewable energy sources, which are characterized by intermittency and variability, but also contributes to the fight against global warming.[4,5] However, the uneven geographical distribution of lithium resources makes it difficult to meet the demand for large-scale electrochemical energy storage and long-term sustainability.[6,7]

As a group I element like lithium, sodium exhibits similar chemical properties, meaning the design concepts established for LIBs can be readily adapted to sodium-ion batteries (SIBs).[8,9] Nevertheless, significant differences exist between the two systems. For example, aluminum can be used as the anode current collector in SIBs, which helps reduce costs.[10,11] On the other hand, conventional graphite anodes are unsuitable for SIBs, with hard carbon emerging as a more appropriate alternative.[4,12] Due to the larger ionic radius of Na^+ ($r = 1.02$ Å) compared to Li^+ ($r = 0.76$ Å), there is greater flexibility in the selection of redox-active transition metal species for layered cathode active materials (CAMs) in SIBs.[7,13,14]

Among the existing CAMs for SIBs, layered oxides have attracted particular attention due to their high theoretical specific capacity and relatively high average working potential.[15,16] Layered oxides based on manganese, represented by $NaMnO_2$ (NMO), have been extensively studied due to the abundance and economic sustainability of manganese.[17,18] However, research into the outgassing of NMO cathodes remains insufficient. In our previous study, we successfully improved the cycling stability of NMO through titanium substitution and, for the first time, investigated its gassing behavior in an electrolyte system consisting of 1 M $NaClO_4$ in a solvent mixture of ethylene carbonate (EC), propylene carbonate (PC), and dimethyl carbonate (DMC) in a volume ratio of 1:1:1, with the addition of 5 vol% fluoroethylene carbonate (FEC).[19]

To gain a deeper understanding of the gas release, in this work, differential electrochemical mass spectrometry (DEMS) was employed for monitoring the electrochemical cycling of NMO in SIB half-cells with six different electrolytes. This approach enables a more comprehensive investigation of gas evolution and provides new insights into the interfacial stability of

S. An, B. Nascimento Nunes, R. Yao, A. Kondrakov, T. Brezesinski
Battery and Electrochemistry Laboratory (BELLA)
Institute of Nanotechnology
Karlsruhe Institute of Technology (KIT)
Kaiserstr. 12, 76131 Karlsruhe, Germany
E-mail: torsten.brezesinski@kit.edu

A. Kondrakov
BASF SE
Carl-Bosch-Str. 38, 67056 Ludwigshafen, Germany

The ORCID identification number(s) for the author(s) of this article can be found under https://doi.org/10.1002/aesr.202500458.

DOI: 10.1002/aesr.202500458

the NMO cathode. In fact, the same CAM was used in this study as in our prior work. Both its structure and electrochemical performance were confirmed to be consistent with previous results; details can be found elsewhere.[19] It should also be noted that the NMO exhibited a secondary particle morphology resulting from the use of a co-precipitated precursor (Mn_3O_4) in the synthesis. This type of morphology is generally beneficial for electrochemical performance.

2. Results and Discussion

To systematically investigate the electrochemical behavior of the NMO cathode in various electrolyte environments, six representative formulations were evaluated. Electrolyte 1 was prepared by dissolving 1 M $NaClO_4$ in a ternary solvent mixture of EC, PC, and DMC in a volume ratio of 1:1:1, with 5 vol% FEC as an additive. Electrolyte 2 used the same EC/PC/DMC solvent system (1:1:1 by volume) with 1 M $NaClO_4$, but without any additives, and thus served as a baseline for elucidating the effect of FEC. Electrolyte 3 consisted of 1 M $NaClO_4$ dissolved in PC, which allowed comparing solvent effects under single-component conditions. To explore the influence of the salt, Electrolytes 4 and 6 were formulated identically to Electrolytes 1 and 3, with the only change being that $NaClO_4$ was replaced by $NaPF_6$. In contrast, Electrolyte 5 was prepared by dissolving 1 M $NaPF_6$ in a binary solvent mixture of EC and DMC (1:1 by volume), allowing for detailed evaluation of the role of PC in affecting the electrochemical performance of the system. The different compositions are summarized in **Table 1** for clarity.

Table 1. Electrolyte formulations investigated in this work.

Electrolyte	Salt	Solvent[s]
1	$NaClO_4$	EC, PC, DMC 1:1:1 by vol., incl. 5 vol% FEC
2	$NaClO_4$	EC, PC, DMC 1:1:1 by vol.
3	$NaClO_4$	PC
4	$NaPF_6$	EC, PC, DMC 1:1:1 by vol., incl. 5 vol% FEC
5	$NaPF_6$	EC, DMC 1:1 by vol.
6	$NaPF_6$	PC

The NMO cathode was first examined in SIB half-cells using each of these electrolytes under identical conditions, with a potential window of 2.0–3.8 V versus Na^+/Na and at a current corresponding to a rate of C/10. The respective first-cycle voltage profiles are presented in **Figure 1** (see Table S1, Supporting Information, for details). In the case of $NaClO_4$-based electrolytes (see Figure 1a–c), Electrolyte 2 exhibited the highest specific charge capacity ($q_{ch} = 269\ mAh\ g^{-1}$), compared to 213 and 207 $mAh\ g^{-1}$ for Electrolytes 1 and 3, respectively. However, the specific discharge capacities and initial Coulomb efficiencies showed opposite trends. Electrolyte 2 delivered only 141 $mAh\ g^{-1}$, corresponding to a Coulomb efficiency of $\varphi \approx 52\%$, whereas Electrolytes 1 and 3 achieved 159 $mAh\ g^{-1}$ (≈75%) and 162 $mAh\ g^{-1}$ (≈78%), respectively. These results suggest that reversible charge storage is more favorable in the presence of either PC or the EC/PC/DMC mixture containing FEC, presumably due to fewer side reactions. In fact, Electrolyte 2 without FEC appeared to suffer from significant parasitic reactions during the charging process. Possible (electro)chemical oxidation and/or reduction reactions that occur in the electrolytes will be discussed later in the section on DEMS.

To explore salt effects, $NaClO_4$ was replaced by $NaPF_6$ and tested under the same electrochemical conditions. As shown in Figure 1d–f, similar trends were observed. The electrolyte with FEC (Electrolyte 4) and the PC-based electrolyte (Electrolyte 6) exhibited comparable first-cycle specific capacities, while the

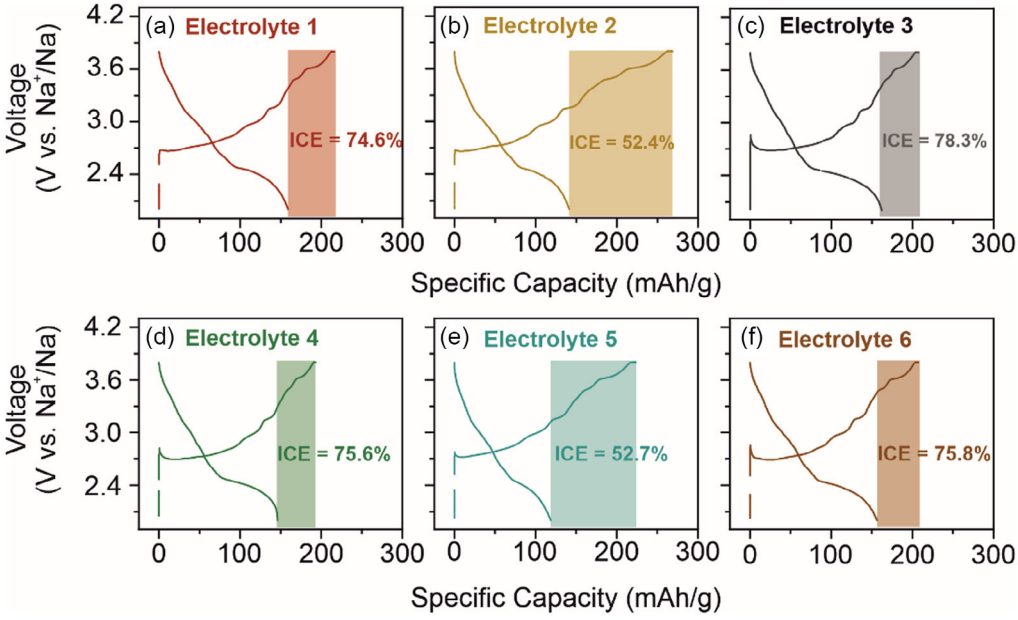

Figure 1. a–f) First-cycle voltage profiles of SIB half-cells with NMO cathode and six representative electrolyte formulations (2.0–3.8 V vs. Na^+/Na, C/10, 25 °C).

EC/DMC system (Electrolyte 5) achieved a lower reversible capacity (with much lower initial Coulomb efficiency). Although substituting the salt led to slightly different performance results, the overall trends remained consistent. Specifically, in the EC/PC/DMC/FEC system, the $NaPF_6$-based electrolyte (Electrolyte 4) resulted in lower specific charge/discharge capacities (193/146 mAh g^{-1}) compared to its $NaClO_4$ counterpart (Electrolyte 1, 213/159 mAh g^{-1}), while the impact of the salt in pure PC (Electrolytes 3 and 6) appeared to be less significant. In the case of Electrolyte 5, which contained only EC and DMC, the NMO cathode experienced severe side reactions similar to those observed with Electrolyte 2. However, the initial specific charge/discharge capacities were even lower than those achieved with Electrolyte 2 (see Table S1, Supporting Information), suggesting that PC likely contributes positively to the overall electrochemical behavior.

In addition, the cycling performance of the NMO cathode over 20 cycles under the same conditions is shown in Figure S1 (Supporting Information). A bar chart comparing capacity retention is presented in Figure S2 (Supporting Information). As evident from this data, Electrolytes 1 and 3 demonstrated similar capacity retention, both around 58%, indicating that $NaClO_4$ with either PC or EC/PC/DMC/FEC exhibits comparable stability in SIB half-cells. A similar finding was made for Electrolytes 1 and 4, although Electrolyte 4 achieved a slightly higher capacity retention (60% vs. 58%). Considering the voltage profiles in Figure 1, these results reveal that although the type of salt plays a certain role in the cycling performance, it is not the decisive factor for the stability of NMO in the EC/PC/DMC/FEC-based systems. Surprisingly, Electrolyte 6 showed the lowest stability with a capacity retention of only 47%, suggesting that $NaClO_4$ is more favorable than $NaPF_6$ in PC-based systems. Electrolytes 2 and 5 also exhibited relatively poor stability, with Electrolyte 5 exhibiting the lowest capacity retention of 52% among them. Overall, it can be concluded that the introduction of PC into the EC/DMC solvent mixture has a positive impact on cell cyclability.

To better understand how the electrolyte formulation affects the cyclability of the NMO cathode, an in situ gas analysis was performed on the different SIB half-cells using DEMS. **Figure 2** and **3** and Table S2 and S3 (Supporting Information) present the results for the six electrolytes, including gas evolution rates and total amounts of evolved oxygen (O_2, $m/z = 32$), hydrogen (H_2, $m/z = 2$), and carbon dioxide (CO_2, $m/z = 44$), as well as the signals at $m/z = 26$ and 28. Ethylene (C_2H_4) is typically detected in fragmented form, with $m/z = 26$ being the most representative fragment, while $m/z = 28$ often originates from a mixture of species, such as C_2H_4, CO, N_2, or CO_2 fragments.[20,21] Since these signals cannot be accurately quantified using calibration gas, their amounts are expressed as ion currents. In general, CO_2 can originate from three main sources, including electrochemical or chemical decomposition of surface carbonates, chemical oxidation of the electrolyte by reactive oxygen, and electrochemical oxidation of the electrolyte at potentials above 4.5 V versus Li^+/Li.[5,7,19,22] H_2 is typically formed from water present in the cell or from protic species generated at high potentials at the cathode side, which subsequently migrate to the anode.[21,23] O_2 is released through irreversible lattice oxygen loss. However, due to its high reactivity, it is often detected in the form of CO_2.[7,24]

For Electrolyte 1 ($NaClO_4$ in EC, PC, DMC 1:1:1 by vol., incl. 5 vol% FEC), shown in the left panel of Figure 2, the gassing behavior has already been reported in considerable detail in

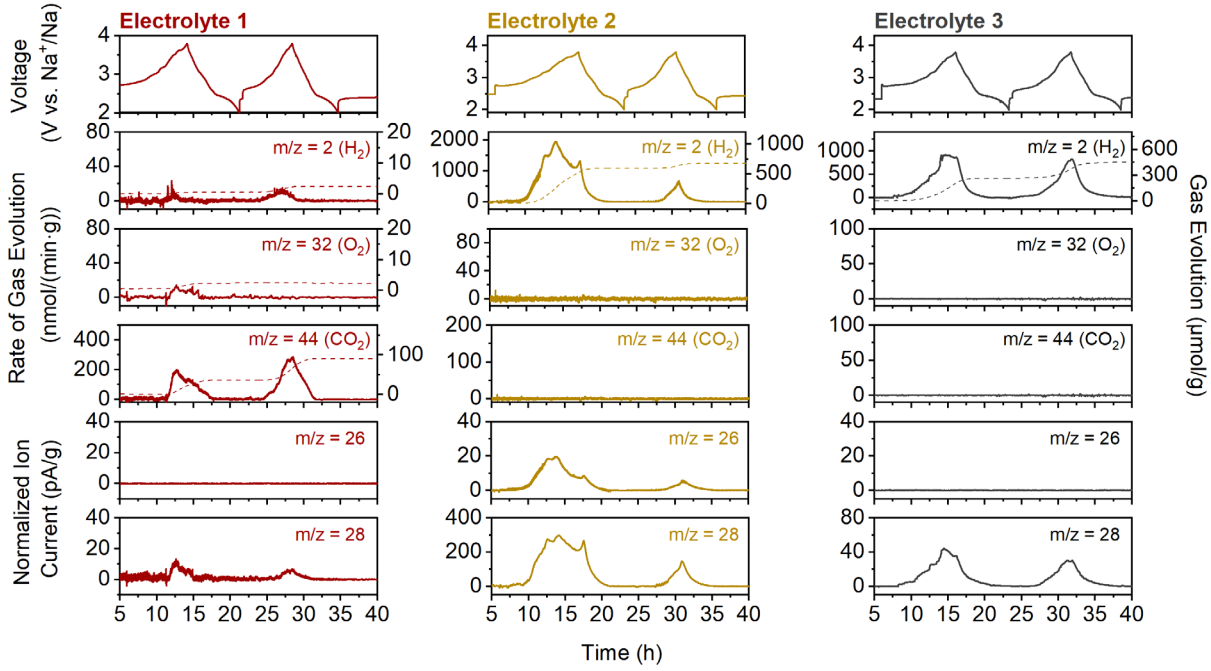

Figure 2. Voltage profiles of SIB half-cells with NMO cathode and various $NaClO_4$-based electrolytes (2.0–3.8 V vs. Na^+/Na, C/10, 25 °C) and corresponding time-resolved evolution rates (left *y*-axis) and cumulative amounts (right *y*-axis) of H_2, O_2, and CO_2, as well as ion currents for $m/z = 26$ and 28 from DEMS.

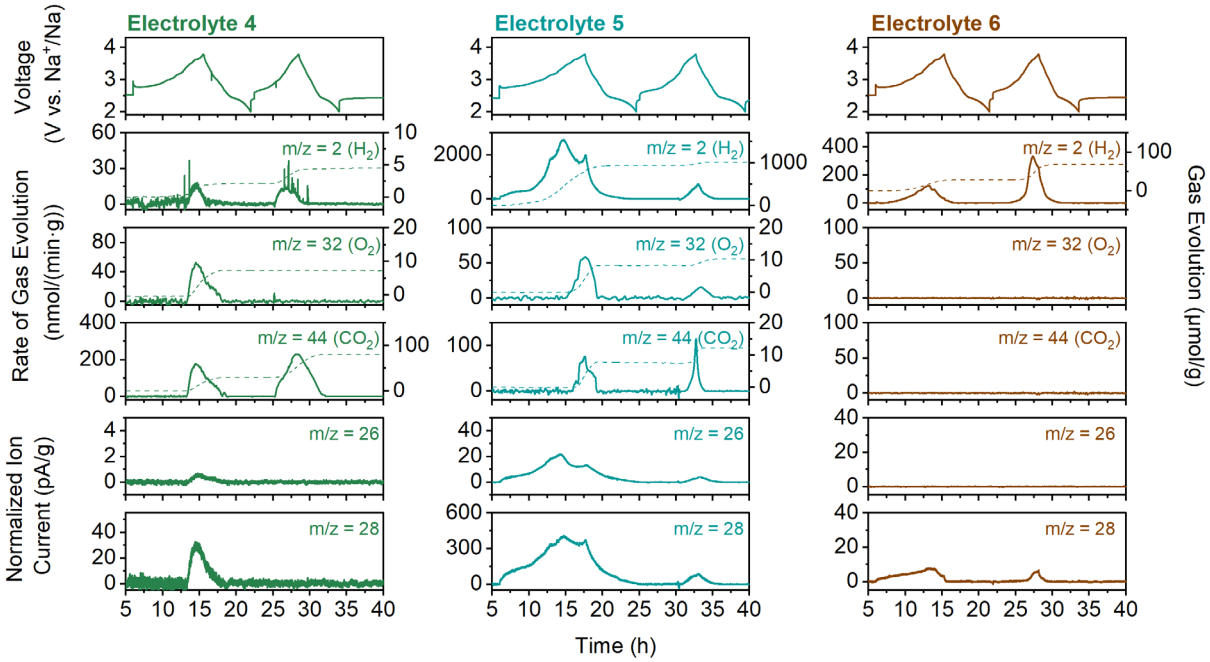

Figure 3. Voltage profiles of SIB half-cells with NMO cathode and various $NaPF_6$-based electrolytes (2.0–3.8 V vs. Na^+/Na, C/10, 25 °C) and corresponding time-resolved evolution rates (left *y*-axis) and cumulative amounts (right *y*-axis) of H_2, O_2, and CO_2, as well as ion currents for $m/z = 26$ and 28 from DEMS.

our previous work.[19] In brief, a small amount of O_2 was detected, which is likely due to irreversible release of lattice oxygen. Notably, gas evolution occurred around 3.25 V versus Na^+/Na, coinciding with the phase transition of NMO to the O1 phase, where oxygen loss may be associated with manganese migration.[25] The detected CO_2 can be attributed to the chemical oxidation of the electrolyte by lattice oxygen and/or the (electro) chemical decomposition of surface carbonates. As described above, the detected H_2 is likely related to the formation of protic species or the presence of residual moisture. No signal corresponding to $m/z = 26$ was observed, indicating that EC did not undergo reductive decomposition to form C_2H_4. In contrast, the $m/z = 28$ signal appeared at an onset potential comparable to that of H_2 and CO_2, suggesting that it may originate from CO_2 fragments or CO.[21,26] However, due to overlapping contributions, a clear assignment cannot be made.

The middle panel of Figure 2 corresponds to Electrolyte 2 ($NaClO_4$ in EC, PC, DMC 1:1:1 by vol.) and shows how the absence of FEC alters the gassing behavior compared to Electrolyte 1. In this case, both the evolution rate and cumulative amount of H_2 increased significantly, as also evident from Table S2 (Supporting Information), and signals at $m/z = 26$ and 28 were detected. In contrast, no release of O_2 or CO_2 was observed, which is somewhat surprising, since one would assume that lattice oxygen loss would lead to measurable amounts of these gases. The absence may be explained by the reaction of released (reactive) oxygen with the electrolyte to produce CO, which is then detected at $m/z = 28$.[24,27] In addition, this finding suggests that the higher CO_2 level for Electrolyte 1 may originate not only from the sources described above, but also from the oxidative and/or reductive decomposition of FEC.[6] Furthermore, the signal at $m/z = 26$ clearly indicates cathodic degradation of EC (C_2H_4 formation), suggesting that it is also involved in the formation of sodium ethylene dicarbonate (NEDC) within the solid-electrolyte interphase (SEI) on the anode.[28,29] Under typical conditions, EC reduction is largely suppressed once a stable SEI has formed.[24] However, in the second cycle, a weak $m/z = 26$ signal was still observed. Therefore, C_2H_4 evolution likely also contributes to the signal at $m/z = 28$. Accordingly, the presence of FEC as an electrolyte additive promotes the formation of a more effective (passivating) SEI. This, in turn, helps mitigate adverse side reactions that would otherwise occur at the anode side.[6,30] The H_2 evolution is probably due to reduction of protic species resulting from electrolyte oxidation, with residual water possibly contributing too.[1] The much higher cumulative amount of released H_2 compared to Electrolyte 1 indicates considerable oxidation, suggesting that FEC may also promote the formation of a cathode-electrolyte interphase (CEI), thereby mitigating (electro) chemical electrolyte degradation. Consequently, the more severe side reactions resulted in a lower initial Coulomb efficiency and poorer capacity retention compared to Electrolyte 1.

The right panel of Figure 2 shows the in situ gas analysis results for the $NaClO_4$-based electrolyte containing only PC as solvent (Electrolyte 3). The data revealed no detectable O_2, CO_2, and $m/z = 26$, while H_2 and $m/z = 28$ signals were clearly observed. Since Electrolyte 3 did not contain EC, the absence of $m/z = 26$ indicates that C_2H_4 formation can be ruled out. Considering the lack of CO_2 evolution and the proven tightness of the DEMS system, this suggests that the signal at $m/z = 28$ is more likely to originate from CO than from N_2 or CO_2 fragments. The formation of CO can be attributed to the anodic decomposition of PC, which is induced by the irreversible release

of lattice oxygen from the NMO cathode, while the pronounced H_2 evolution is again explained by the reduction of protic species and/or residual water. In addition, PC can also be reduced on the anode to form sodium propylene dicarbonate (NPDC). We note that NPDC is more soluble in the electrolyte than NEDC and can migrate to the cathode, where it may undergo further oxidation reactions.[28] Nevertheless, despite the occurrence of these parasitic reactions, the specific capacities in the first cycle, the initial Coulomb efficiency, and the cycling stability were similar to those of Electrolyte 1 (see Table S1, Supporting Information). It has been reported that this is due to the formation of a robust SEI in the $NaClO_4$/PC-based system, which stabilizes the electrodelelectrolyte interface.[31] It is also worth mentioning that in DMC-containing electrolytes, the higher stability of DMC against reactive oxygen and the use of a relatively low upper cut-off potential (3.8 V vs. Na^+/Na) mean that its (electro)chemical oxidation only makes a minor contribution.[2]

Figure 3 shows the gassing behavior after replacing $NaClO_4$ with $NaPF_6$. When comparing Electrolytes 1 and 4, it becomes clear that the general evolution profiles are similar, although the total amounts of individual gases differ. As summarized in Table S2 (Supporting Information), Electrolyte 4 ($NaPF_6$ in EC, PC, DMC 1:1:1 by vol., incl. 5 vol% FEC) exhibited a slightly lower CO_2 release than Electrolyte 1, whereas the evolution rates and cumulative amounts of the other gases were higher. The increase in H_2 evolution is likely related to the HF generated by the decomposition of $NaPF_6$.[6,32] At the same time, the higher evolution rate of O_2 may be due to HF-induced manganese dissolution (rather than differences in state of charge), which facilitates lattice oxygen loss.[33] The appearance of a weak signal at $m/z = 26$ suggests minor EC decomposition. The slight reduction in CO_2 evolution may also be explained by the presence of HF, which increases the acidity of the electrolyte and suppresses OH^--induced hydrolysis of EC and/or PC.[21,34] Furthermore, the formation of a CEI is believed to help passivate interfacial reactions, thereby reducing the evolution of CO_2.[28,29] Similarly, the preferred reduction of FEC leads to the formation of NaF, which contributes to the construction of a stable SEI.[31] This stabilizing effect prevents additional side reactions, e.g., with the PC. Overall, differences in salt type only have a limited impact on the electrochemical performance and gassing behavior of the NMO cathode in SIB half-cells using the EC/PC/DMC/FEC systems (Electrolytes 1 and 4).

The middle panel of Figure 3 presents the DEMS data for Electrolyte 5, in which both FEC and PC were absent. This formulation enabled a more focused investigation into the specific role of PC within the system. Compared to Electrolyte 2, which contained PC, Electrolyte 5 showed clear signals of O_2 and CO_2 release. In contrast, the evolution profile of H_2, as well as those for $m/z = 26$ and 28, was comparable to that of Electrolyte 2. However, a higher cumulative amount of released H_2 (and $m/z = 28$) was observed for Electrolyte 5, suggesting that PC likely alters, to some extent, the anodic degradation behavior of the EC/DMC-based system. However, the role of HF in this

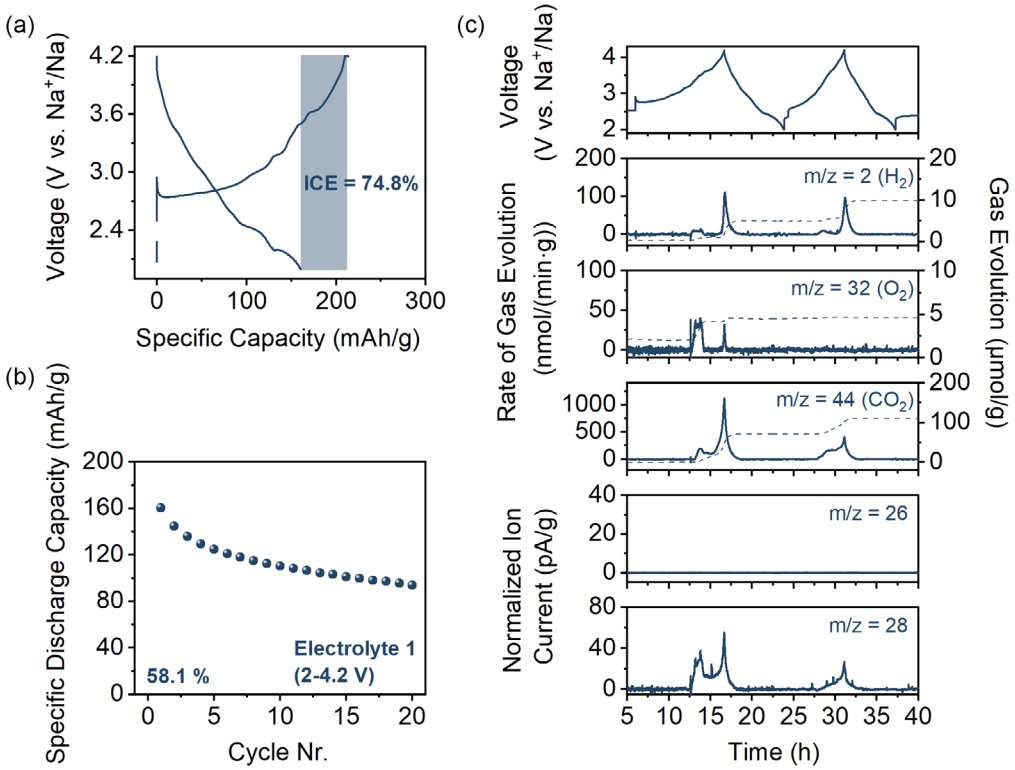

Figure 4. a) First-cycle voltage profiles, b) cycling performance, and c) gassing behavior of SIB half-cells with NMO cathode and $NaClO_4$-based electrolyte (2.0–4.2 V vs. Na^+/Na, C/10, 25 °C). Time-resolved evolution rates (left *y*-axis) and cumulative amounts (right *y*-axis) of H_2, O_2, and CO_2, as well as ion currents for $m/z = 26$ and 28 from DEMS, are shown in panel c).

context remains largely unclear. In addition, notable differences in CO_2 evolution were observed between Electrolytes 4 and 5. While CO_2 release was still detectable for Electrolyte 5 without PC, the evolution rate and cumulative amount were significantly lower than for Electrolyte 4. This again supports the conclusion that a larger proportion of the CO_2 originates from the decomposition of FEC.

When PC is used as the only solvent (Electrolytes 3 and 6), regardless of the salt, as shown in the right panels of Figure 2 and 3, signals at $m/z = 2$ and 28 were consistently observed. This suggests that gas evolution is not merely a linear combination of the decomposition of individual electrolyte components, but rather the result of unique interactions between different solvents and salts. Such synergistic effects help reduce electrolyte degradation during cycling. Furthermore, the presence of PC appears to suppress the direct evolution of both O_2 and CO_2, suggesting that oxygen released from the CAM preferentially reacts with PC to produce CO, thereby altering the gas composition. Although Electrolyte 6 did not exhibit a particularly strong gas evolution profile, its electrochemical performance was less satisfactory. Since $NaPF_6$ is the only variable in Electrolyte 6, it is likely the main factor. Unlike EC, PC alone cannot form an effective passivation layer, resulting in continuous PC decomposition during battery operation and thus poorer stability.[28,31] Apart from that, the introduction of $NaPF_6$ inevitably leads to the formation of HF, which accelerates the dissolution of manganese from NMO and further impairs cell cyclability.[33] Note that prior studies have reported that in PC-based electrolytes, $NaClO_4$ can form a more uniform and stable SEI compared to $NaPF_6$. This helps explain the enhanced cycling performance of Electrolyte 3 compared to Electrolyte 6.[31]

Since Electrolyte 1 showed the best overall performance among the six electrolytes employed in this work, it was further tested with a higher upper cutoff potential of 4.2 versus Na^+/Na, as shown in **Figure 4**. As can be seen, the evolution rates of H_2 and CO_2 in particular increased sharply with increasing cutoff potential during charging (see Figure 4c and Table S2, Supporting Information), with the most intense gas release observed near 4.2 V. This result therefore suggests that a higher upper cutoff potential leads to a greater degradation of the electrolyte, which is in line with expectations. Surprisingly, however, the different gassing behavior had no immediate effect on the cycling performance of the respective SIB half-cells over the first 20 cycles (see Figure 4a,b and Table S1, Supporting Information). We assume that long-term cycling is necessary to detect discernible differences in stability.

3. Conclusion

In summary, this study compared the cyclability and gassing behavior of SIB half-cells with NMO cathode and various $NaClO_4$- and $NaPF_6$-based electrolytes. It is found that systems containing EC, PC, and DMC as solvents and FEC as an additive exhibit minimal gas evolution and favorable electrochemical performance, regardless of whether $NaClO_4$ or $NaPF_6$ is used. This is primarily due to the formation of a robust SEI and/or CEI in the presence of FEC. Furthermore, the use of $NaClO_4$ with PC as the sole solvent also enables relatively good cyclability. In contrast, the addition of EC without FEC leads to increased gas release, accompanied by a deterioration in performance, regardless of the salt. Aside from that, for the EC/PC/DMC/FEC-based system with $NaClO_4$, the upper cutoff potential is shown to determine the rates of gas evolution and cumulative amounts, while it has only a minor effect on SIB performance and stability over the first 20 cycles.

4. Experimental Section

Synthesis: The $NaMnO_2$ cathode active material was prepared by a single-step solid-state synthesis method. Specifically, Mn_3O_4 ($d_{50} \approx$ 14 µm, BASF Shanshan Battery Materials Co. Ltd.) and Na_2CO_3 (99.9%, Sigma-Aldrich) were weighed in a molar ratio of 1:1.05 and thoroughly mixed for 10 min under Ar atmosphere using a high-speed laboratory blender (Kinematica) to ensure homogeneity. The resulting powder blend was then placed into an alumina crucible and subjected to calcination at 800 °C for 12 h in a tubular furnace (Nabertherm RHTC80/230/16) under a continuous flow of air (7 L h^{-1}). The temperature was increased at a rate of 5 K min^{-1}. After thermal treatment, the samples were rapidly cooled to room temperature.

Battery Testing: The electrodes were prepared by casting a slurry containing 80 wt% $NaMnO_2$ cathode active material, 10 wt% Super C65 as a conductive carbon additive, and 10 wt% polyvinylidene difluoride (PVDF, Solef 5130, Solvay) as the binder, all dispersed in N-methyl-2-pyrrolidone (NMP). The slurry was homogenized using a planetary centrifugal mixer (Thinky ARE-250) at sequential speeds of 2000 and 400 rpm for a total of 6 min. The resulting slurry was then coated onto 30 µm-thick aluminum foil, serving as the current collector, using a film applicator (Erichsen Coatmaster 510) at a rate of 5 mm s^{-1}. After coating, the cathode sheets were dried in a dynamic vacuum at 120 °C and subsequently compacted using a roll press (Sumet Messtechnik) at a line pressure of 14 N mm^{-1} to increase electrode density. Finally, circular electrodes of diameter 13 mm and with areal mass loadings of (6 ± 1) mg cm^{-2} were punched out for cell assembly.

CR2032 coin cells were assembled in an Ar glovebox using sodium metal as counter and reference electrodes, GF/D glass fiber as separator, and 95 µL of electrolyte. A battery cycler from MACCOR Inc. was used for electrochemical testing via galvanostatic cycling in a potential window of 2.0–3.8 or 4.2 V versus Na^+/Na, with a constant voltage step at the upper cutoff potential, either for 30 min or until the current decreased below C/100, and with 1C being defined as 200 mA g^{-1}.

Differential Electrochemical Mass Spectrometry: DEMS measurements were performed on customized SIB half-cells with cathodes of 30 mm in diameter and areal mass loadings of about 10 mg cm^{-2} using 700 µL of electrolyte. Electrochemical cycling was performed at a rate of C/10. A continuous flow of helium (purity grade 6.0, 2.5 mL min^{-1}) as a carrier gas was maintained through the cells. The evolved gases were extracted in real-time and analyzed using a mass spectrometer (OmniStar GSD 320, Pfeiffer Vacuum GmbH).

Supporting Information

Supporting Information is available from the Wiley Online Library or from the author.

Acknowledgements

This study was supported by BASF SE. T. B. and B. N. N are grateful to the Federal Ministry of Research, Technology, and Space (BMFTR) for funding within the project ENTISE (03XP0579K).

Open Access funding enabled and organized by Projekt DEAL.

Conflict of Interest

The authors declare no conflict of interest.

Data Availability Statement

The data that support the findings of this study are available from the corresponding author upon reasonable request.

Keywords

differential electrochemical mass spectrometry, (electro)chemical degradation, gas analysis, interfacial stability

Received: November 4, 2025
Revised: December 18, 2025
Published online:

[1] M. Metzger, B. Strehle, S. Solchenbach, H. A. Gasteiger, *J. Electrochem. Soc.* **2016**, *163*, A798.
[2] A. T. S. Freiberg, M. K. Roos, J. Wandt, R. de Vivie-Riedle, H. A. Gasteiger, *J. Phys. Chem. A* **2018**, *122*, 8828.
[3] Y.-X. Chang, L. Yu, X. Xing, Y.-J. Guo, Z.-Y. Xie, S. Xu, *Chem. Rec.* **2022**, *22*, e202200122.
[4] X. Deng, Y. Huang, Y. Han, J. Du, J. Tian, Y. Li, Y. Yu, Y. Shen, Y. Huang, *Angew. Chem., Int. Ed.* **2024**, *63*, e202412222.
[5] S. An, L. Karger, P. Müller, J. Lin, S. Vasala, V. Baran, S. L. Dreyer, R. Zhang, F. Ulusoy, A. Kondrakov, J. Janek, T. Brezesinski, *Chem. Eng. J.* **2025**, *509*, 160939.
[6] L. Zhang, C. Tsolakidou, S. Mariyappan, J.-M. Tarascon, S. Trabesinger, *Energy Storage Mater.* **2021**, *42*, 12.
[7] S. An, L. Karger, S. L. Dreyer, Y. Hu, E. Barbosa, R. Zhang, J. Lin, M. Fichtner, A. Kondrakov, J. Janek, T. Brezesinski, *Mater. Futures* **2024**, *3*, 035103.
[8] K. Chayambuka, G. Mulder, D. L. Danilov, P. H. L. Notten, *Adv. Energy Mater.* **2018**, *8*, 1800079.
[9] R.-M. Gao, Z.-J. Zheng, P.-F. Wang, C.-Y. Wang, H. Ye, F.-F. Cao, *Energy Storage Mater.* **2020**, *30*, 9.
[10] Y. Zhang, R. Zhang, Y. Huang, *Front. Chem.* **2019**, *7*, 335.
[11] R. J. Clément, P. G. Bruce, C. P. Grey, *J. Electrochem. Soc.* **2015**, *162*, A2589.
[12] K. Kubota, S. Komaba, *J. Electrochem. Soc.* **2015**, *162*, A2538.
[13] S. Li, Y. Sun, Y. Pang, S. Xia, T. Chen, H. Sun, S. Zheng, T. Yuan, *Asia-Pac. J. Chem. Eng.* **2022**, *17*, e2762.
[14] K. Tian, Y. Dang, Z. Xu, R. Zheng, Z. Wang, D. Wang, Y. Liu, Q. Wang, *Energy Storage Mater.* **2024**, *73*, 103841.
[15] S. Guo, H. Yu, P. Liu, Y. Ren, T. Zhang, M. Chen, M. Ishida, H. Zhou, *Energy Environ. Sci.* **2015**, *8*, 1237.
[16] P.-F. Wang, Y. You, Y.-X. Yin, Y.-S. Wang, L.-J. Wan, L. Gu, Y.-G. Guo, *Angew. Chem., Int. Ed.* **2016**, *128*, 7571.
[17] X. Chen, Y. Wang, K. Wiaderek, X. Sang, O. Borkiewicz, K. Chapman, J. LeBeau, J. Lynn, X. Li, *Adv. Funct. Mater.* **2018**, *28*, 1805105.
[18] X. Ma, H. Chen, G. Ceder, *J. Electrochem. Soc.* **2011**, *158*, A1307.
[19] S. An, R. Sahu, R. Zhang, F. Ulusoy, C. Kübel, A. Kondrakov, J. Janek, T. Brezesinski, *ACS Appl. Energy Mater.* **2025**, *8*, 10508.
[20] B. B. Berkes, A. Jozwiuk, H. Sommer, T. Brezesinski, J. Janek, *Electrochem. Commun.* **2015**, *60*, 64.
[21] S. L. Dreyer, A. Kondrakov, J. Janek, T. Brezesinski, *J. Mater. Res.* **2022**, *37*, 3146.
[22] F. Strauss, S. Payandeh, A. Kondrakov, T. Brezesinski, *Mater. Futures* **2022**, *1*, 023501.
[23] B. Zhou, S. An, D. Kitsche, S. L. Dreyer, K. Wang, X. Huang, J. Thanner, M. Bianchini, T. Brezesinski, B. Breitung, H. Hahn, Q. Wang, *Small Struct.* **2024**, *5*, 2400005.
[24] R. Jung, M. Metzger, F. Maglia, C. Stinner, H. A. Gasteiger, *J. Electrochem. Soc.* **2017**, *164*, A1361.
[25] K. Kubota, M. Miyazaki, E. J. Kim, H. Yoshida, P. Barpanda, S. Komaba, *J. Mater. Chem. A* **2021**, *9*, 26810.
[26] B. B. Berkes, A. Jozwiuk, M. Vračar, H. Sommer, T. Brezesinski, J. Janek, *Anal. Chem.* **2015**, *87*, 5878.
[27] R. Jung, M. Metzger, F. Maglia, C. Stinner, H. A. Gasteiger, *J. Phys. Chem. Lett.* **2017**, *8*, 4820.
[28] T. Melin, R. Lundström, E. J. Berg, *Adv. Mater. Interfaces* **2022**, *9*, 2101258.
[29] S. Solchenbach, G. Hong, A. T. S. Freiberg, R. Jung, H. A. Gasteiger, *J. Electrochem. Soc.* **2018**, *165*, A3304.
[30] R. Jung, M. Metzger, D. Haering, S. Solchenbach, C. Marino, N. Tsiouvaras, C. Stinner, H. A. Gasteiger, *J. Electrochem. Soc.* **2016**, *163*, A1705.
[31] A. Darwiche, L. Bodenes, L. Madec, L. Monconduit, H. Martinez, *Electrochim. Acta* **2016**, *207*, 284.
[32] A. T. S. Freiberg, J. Sicklinger, S. Solchenbach, H. A. Gasteiger, *Electrochim. Acta* **2020**, *346*, 136271.
[33] D. R. Gallus, R. Schmitz, R. Wagner, B. Hoffmann, S. Nowak, I. Cekic-Laskovic, R. W. Schmitz, M. Winter, *Electrochim. Acta* **2014**, *134*, 393.
[34] M. Metzger, B. Strehle, S. Solchenbach, H. A. Gasteiger, *J. Electrochem. Soc.* **2016**, *163*, A1219.